

1 *Communication*

# 2 **Room-Temperature H<sub>2</sub> Gas Sensing Characterization** 3 **of Graphene-doped Porous Silicon via a Facile** 4 **Solution Dropping Method**

5 **Nu Si A Eom<sup>†</sup>, Hong-Baek Cho<sup>†</sup>, Yoseb Song<sup>1</sup>, Woojin Lee<sup>2</sup>, Tohru Sekino<sup>3</sup> and Yong-Ho Choa<sup>1\*</sup>**

6 <sup>1</sup> Department of Fusion Chemical Engineering, Hanyang University, Ansan, 15588, Republic of Korea.

7 <sup>2</sup> Process Development Team, Semiconductor R&D Center, Samsung Electronics Co., LTD, Samsungjeonja-  
8 ro 1, Hwaseong, Gyeonggi-do 445-330, Republic of Korea

9 <sup>3</sup> The Institute of Scientific and Industrial Research, Osaka University, 8-1 Mihogaoka, Ibaraki, Osaka, 567-  
10 0047, Japan

11  
12 † These authors contributed equally to this work

13  
14 \* Correspondence: choa15@hanyang.ac.kr; Tel.: +82-31-400-5650

15  
16  
17 **Abstract:** In this study, a graphene-doped porous silicon (G-doped/p-Si) substrate for low ppm H<sub>2</sub>  
18 gas detection by an inexpensive synthesis route was proposed as a potential noble graphene-based  
19 gas sensor material and to understand the sensing mechanism. The G-doped/p-Si gas sensor was  
20 synthesized by a simple capillary force-assisted solution dropping method on p-Si substrates,  
21 whose porosity was generated through an electrochemical etching process. G-doped/p-Si was  
22 fabricated with various graphene concentrations and exploited as a H<sub>2</sub> sensor operated at room  
23 temperature. The sensing mechanism of the sensor with/without graphene decoration on p-Si was  
24 proposed to elucidate the synergetic gas sensing effect generated from the interface between the  
25 graphene and p-type silicon.

26  
27 **Keywords:** graphene-doped porous silicon; p-type silicon; hydrogen sensor; sensing mechanism

## 28 29 30 **1. Introduction**

31 Hydrogen gas is widely used as a clean fuel in various industrial fields and is expected to be  
32 the fuel to replace fossil fuels [1]. Since H<sub>2</sub> is known to be highly colorless, odorless, and explosive  
33 at concentrations greater than 4% [2], the ability to detect early hydrogen leakage is prerequisite  
34 and demand for a highly sensitive H<sub>2</sub> gas sensor is increasing. In general, gas sensors are of great  
35 interest because of their ability for real time analysis of gaseous chemicals over a wide range of  
36 applications. In the vast area of gas sensing, hydrogen sensors are based on metal oxide films  
37 configured in a chemiresistor mode [3]. Typical metal oxide gas sensors have high power  
38 consumption due to their high working temperatures (200-400°C) [4]. Compared to other  
39 semiconductor gas sensors, a porous silicon (p-Si) gas sensor can be operated at relatively low  
40 temperatures, even at room temperature [5]. p-Si is an interesting base material with which to  
41 develop a gas sensor due to their unique combination of crystalline structure, high specific surface  
42 area, and high surface chemical activity [6]. Various additives have been incorporated into p-Si to  
43 enhance its sensing property [7] because the response is dependent on the base device matrix and  
44 the influence of catalytic components like Pd, Pt, and Ru. [8].

45 Gas sensing is one of the most promising applications for graphene because the delocalized  
46  $\pi(p)$  bonds of graphene allow charge carriers to have zero rest mass and high mobility [9, 10], and  
47 graphene has high surface-to-volume ratio and high surface chemical activity for enhanced  
48 adsorption of gases on the basal surface [11]. Graphene is utilized as a matrix material for the sensor  
49 of a general graphene-based gas sensor, which can be easily synthesized by the incorporation of  
50 other supportive sensor materials like metal oxides [12]. The operational principle of such graphene  
51 devices is based on changes in their electrical conductivity due to gas molecules adsorbed on the  
52 graphene surface acting as donors or acceptors, similar to other solid-state sensors [13,14].  
53 However, to the best of our knowledge, there have been no studies that have investigated the gas  
54 sensing property describing incorporation of a graphene decoration on a p-Si matrix.

55 In this study, the sensor properties for low ppm  $H_2$  gas detection based on graphene-doped  
56 porous silicon (G-doped/p-Si) substrate are investigated utilizing graphene as a catalyst material.  
57 Graphene doping was performed by a facile, inexpensive synthetic procedure using solution  
58 dropping onto a p-Si substrate with a one-step method of decorating graphene on the high surface  
59 area porous media created via an electrochemical etching process. Electrochemical etching is  
60 typically a simple, inexpensive procedure that allows operators a sufficiently free hand when  
61 synthesizing p-Si layers [6]. The loaded amount of graphene was varied as a function of graphene  
62 concentration ranging from 0 to 10 mg/ml in an aqueous solution, whose potential as a hydrogen  
63 gas sensor was evaluated during operation at room temperature. Drawing on graphene's intrinsic  
64 properties of high mobility and conductivity, attention was focused on exploring the role of the  
65 formation of the electrical junction between graphene-to-silicon interfaces for the enhancement of  
66 hydrogen gas detection.

## 67 2. Materials and Methods

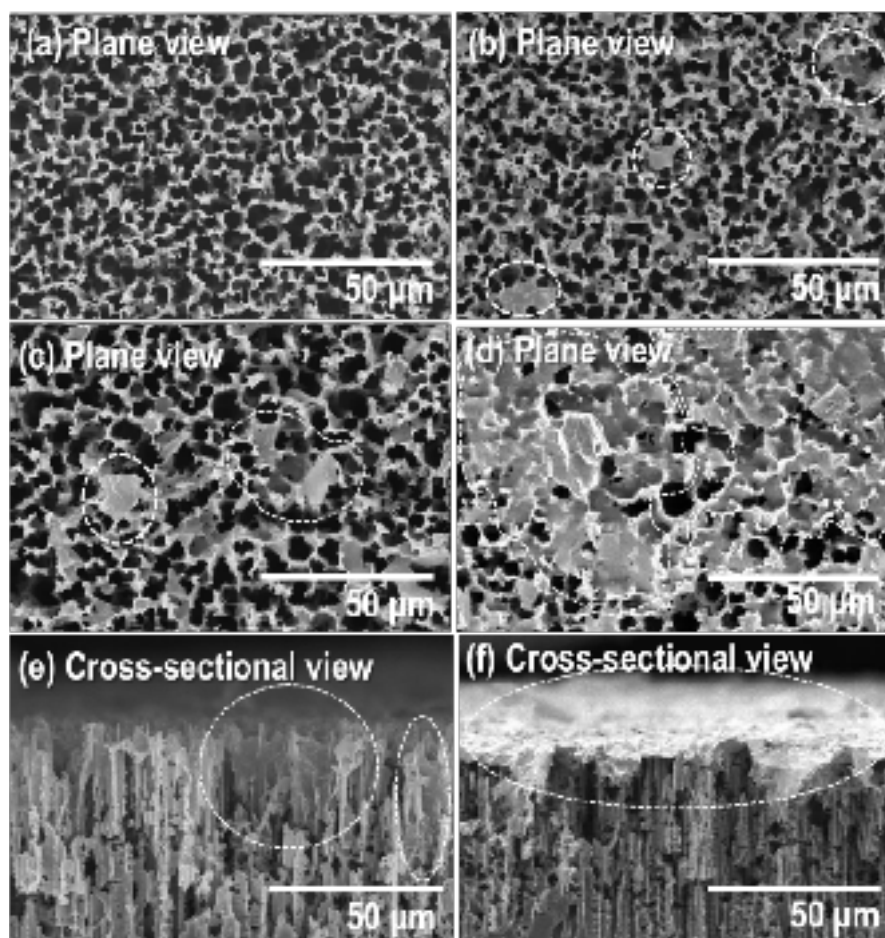
68 **2.1 Material.** Water-dispersible graphene was developed by MExplorer Co., Ltd., the thickness  
69 and lateral dimension of the as-received graphene was  $< 5$  nm and 2-3  $\mu$ m, respectively [See Fig.  
70 S1].

71 **2.2 Synthesis of the p-Si substrate.** The synthesis of the high porosity silicon substrate was  
72 performed by a technique combining both metal-assisted chemical etching (MacE) and  
73 electrochemical etching [15] utilizing a p-type monocrystalline silicon wafer with a 300  $\mu$ m  
74 thickness,  $\langle 100 \rangle$  orientation and 1-10  $\Omega$  resistance. To conduct the MacE process, Pt-catalyst loading  
75 on the prepared porous silicon was performed by the sputter process (Quorum Technologies,  
76 Q150T, ES) utilizing the Pt (purity: 99.99%) target. The domains of the deposited Pt metal particles  
77 with a nano-dimension ranging from 30 to 60 nm were formed on the Si substrate after deposition  
78 and heat treatment at 650°C. After cooling to room temperature, the Pt particle-doped silicon wafer  
79 was attached to aluminum foil for electrochemical etching. The silicon substrate and Pt electrode  
80 were connected to a DC power supply (E3647A, Agilent) as a working electrode and counter  
81 electrode, respectively, that were computer controlled. A current density of 1 mA/cm<sup>2</sup> was applied  
82 for 1h in a mixture solution of 30 wt%  $H_2O_2$  and 10 wt% HF. After the chemical etching, the porous  
83 silicon substrate was dipped in 10 wt% HF to remove the formed oxide layer from the silicon  
84 surface for the electrochemical etching processes, and the samples were then rinsed copiously in DI  
85 water and dried at room temperature.

86 **2.3 Synthesis of graphene-doped porous silicon heterostructure.** Doping graphene on the  
87 synthesized p-Si substrate was performed by a facile solution drop method using a micro pipet. The  
88 100  $\mu$ l solution volume as a function of graphene concentration ranging from 0 to 10 mg/ml in an  
89 aqueous solution on the p-Si substrate size (5  $\times$  10 mm<sup>2</sup>) was deposited and dried for 20 min in  
90 atmosphere at 100°C. The morphology of the Pd-doped p-Si was analyzed using a scanning electric  
91 microscope (SEM, MIRA3, TESCAN Ltd., USA). A 200-nm thick gold layer for the sensor electrode  
92 was evaporated on the top of each p-Si surface to create the electrical contact. The formed electrode  
93 and  $H_2$  sensing properties of the sensor system were measured at room temperature and recorded  
94 online by a NI PXle-1073 (National Instruments Corporation, USA).

95

## 96 3. Results

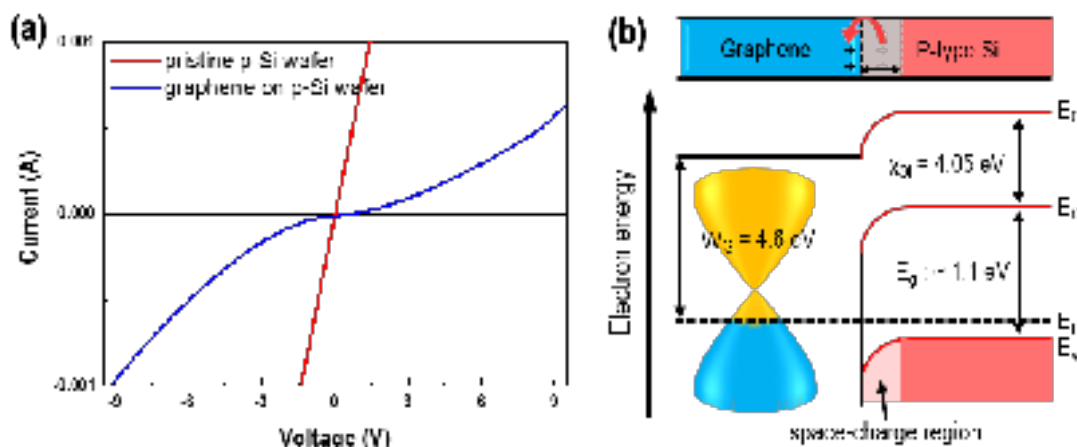


97

98 **Figure 1.** Plane and cross-sectional SEM images of the G-doped/p-Si with (a) 0, (b) 0.1, (c), (e) 1, and  
 99 (d), (f) 10 mg/ml graphene solution concentrations.

100 Figure 1 shows the SEM image of the G-doped/p-Si dried after doping 100  $\mu$ l of the graphene  
 101 solution on p-Si substrate. The loaded amount of graphene on the p-Si wafer substrate was  
 102 increased as the concentration of graphene increased from 0 to 10 mg/ml. The size of the graphene  
 103 identified from the SEM view (the dotted domains) ranged from several to tens of microns. The  
 104 external average pore size of the synthesized p-Si is 4.5  $\mu$ m macroporosity, whose width narrows  
 105 to meso- and micro-porosity toward a vertical hole depth of approximately 90  $\mu$ m [see Fig. S2],  
 106 which could be confirmed by the nano-dimensional cracks on the inside wall of the p-Si [see Fig. S2  
 107 inset]. This porous structure enables the decoration of graphene 2-3  $\mu$ m inside the surface. Upon  
 108 adding the graphene solution drop-wise to the surface, it diffused into the p-Si by capillary force  
 109 [16] from the lateral dimension of the as-received graphene. In spite of this, when the concentration  
 110 of the graphene increases, a larger amount of graphene appears on the external surface of the p-Si  
 111 [Figs. 1(a)-(d)] and on the internal porous wall near the silicon surface (Fig. 1(e)). The majority of  
 112 the external surface was then covered by graphene when the graphene concentration reached 10  
 113 mg/ml, as shown in Fig. 1(f). Thus, the sensing properties can be tuned if a heterojunction created  
 114 between the decorated graphene-to-silicon interface occurs throughout the extended p-Si surfaces.  
 115

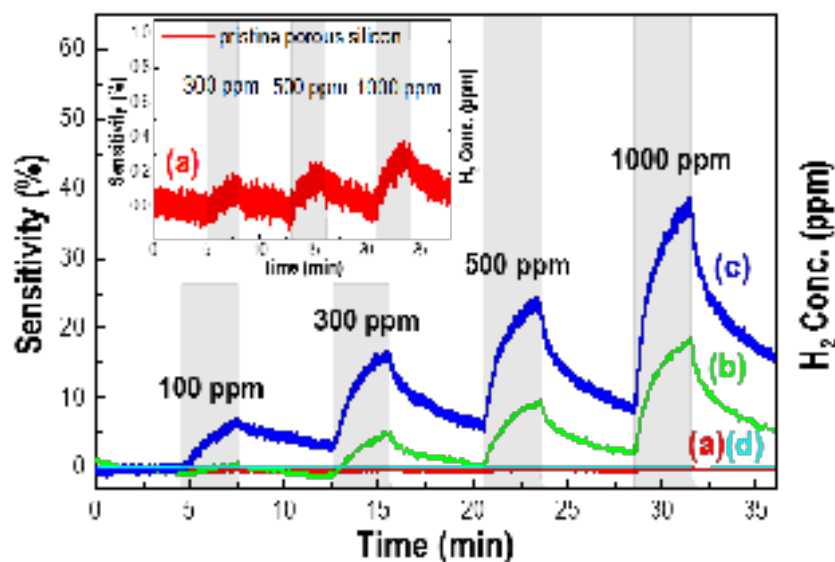
4 of 7



116

117 **Figure 2.** (a) IV curve and (b) junction schematic of a pristine p-Si wafer and G-doped/p-Si sensors  
 118 at room temperature.

119 Figure 2 shows the IV behaviors and energy band diagrams of pristine and graphene-  
 120 deposited p-Si that confirms the creation of a heterojunction between the p-type Si of the  
 121 semiconductor and graphene of the semi-metal with deposited graphene on the pristine p-Si. This  
 122 can be consulted from the report describing the formation of the Schottky barrier at the  
 123 graphene/silicon interface [17], the partial carriers in p-type silicon tends to move to the graphene  
 124 (Fig. 2-a) and consequently, the energy levels near the silicon surface will bend downward (Fig.2-b)  
 125 facilitating the formation of a space-charge region and built-in electric field near the  
 126 graphene/silicon interface due to the work function of graphene (4.6 eV) more than p-type silicon.  
 127 Therefore, the IV curve shows that with and without graphene deposited, p-Si has ohmic and  
 128 Schottky junctions, respectively.



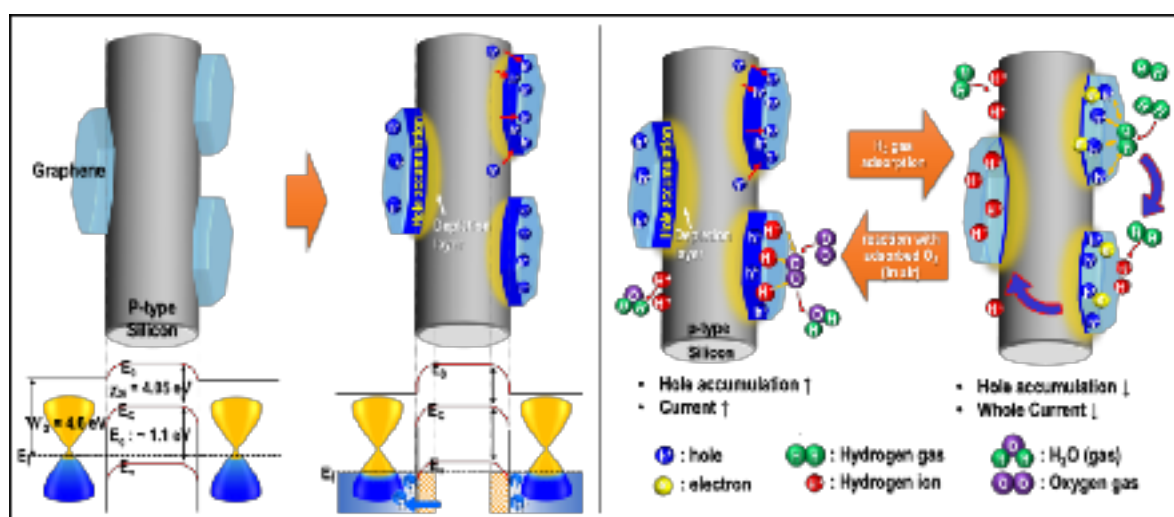
129

130 **Figure 3.** Response of a pristine p-Si wafer (thickness 70  $\mu\text{m}$ ) and G-doped/p-Si sensors with (a) 0,  
 131 (b) 0.1, (c) 1, and (d) 10 mg/ml graphene concentrations to an air-based  $\text{H}_2$  gas operated at room  
 132 temperature.

133 Figure 3 shows the  $\text{H}_2$  sensing properties of the G-doped/p-Si as a function of graphene  
 134 concentration at room temperature. The pristine p-Si wafer has little sensing property for hydrogen  
 135 molecules with sensitivity less than 0.5 % under 100 to 1000 ppm  $\text{H}_2$  at a flow rate of 500 sccm [see  
 136 Fig. 3(a)] and also the inset), whereas the p-Si with graphene has an obvious increase in sensing  $\text{H}_2$   
 137 gas with a concentration ranging from 100 to 1000 ppm (Fig. 3(b)). The sensing property of p-Si



138 with doped graphene increased with an increase in H<sub>2</sub> gas concentration as well as graphene  
 139 solution concentration. Hydrogen gas can be adsorbed on the surface of p-type silicon, where the  
 140 gas molecules extract holes from the adsorbed surface of silicon that could form ionized hydrogen  
 141 by the hydrogen redox reaction [17] contributing to very weak variation of sensitivity, as shown in  
 142 the inset of Fig. 3. Moreover, as described in Fig. 2 over G-doped/p-Si, the major carrier (hole)  
 143 originated from the p-type silicon transfers to graphene and motivates the adsorption of the  
 144 hydrogen gas molecule. Thus, the G-doped silicon surface enhances the sensing property in  
 145 comparison to the pristine p-Si substrate, drawing on the type of adsorbed gas molecules on the  
 146 graphene surface that act as donors or acceptors [18]. On the other hand, for the surface of p-Si with  
 147 1 mg/ml doped graphene, the majority of the porosity was covered by graphene (Fig. 1(f)),  
 148 exhibiting a very low sensitivity similar to pristine p-Si (Fig. 3(d)). The G-doped/p-Si does not have  
 149 a sensing property because p-Si hinders the diffusion of H<sub>2</sub> gas to the active site of graphene-silicon  
 150 located deep inside the porous wall, and the current flow paths are generated only from the  
 151 graphene surface.  
 152



153

154 **Figure 4.** Schematic illustration showing the adsorption and desorption mechanism of H<sub>2</sub> gas on the  
 155 surface of doped-graphene on a p-Si wafer.

156 Figure 4 shows the band diagram between graphene and p-type silicon. Graphene has a lower  
 157 work function than p-type silicon 4.6 eV ( $W_G = 4.6$  eV) and p-type silicon has an electron affinity of  
 158 4.05 eV ( $\chi_{Si}$ ) and a band gap of  $\sim 1.1$  eV ( $E_g$ ), causing a Schottky junction due to contact between  
 159 graphene and p-type silicon [19]. When the junction is generated between graphene and p-type  
 160 silicon, the major carrier of p-type silicon moves to graphene due to the disparity in work function,  
 161 forming an electric depletion layer near the p-type silicon and the hole accumulation layer near the  
 162 graphene [20]. The electric depletion layer was formed over a wide internal surface area of the p-Si  
 163 substrate with a large specific area. Upon adsorption of hydrogen gas molecules to the surface of G-  
 164 doped/p-Si, the accumulated holes near the graphene react with hydrogen molecules, which could  
 165 form ionized hydrogen by the hydrogen redox reaction  $H_2 + 2h^+ \rightarrow 2H^+$ , resulting in a reduction in  
 166 the carrier density [17]. The conduction of G-doped/p-Si decreased due to the decreased graphene  
 167 carrier concentration. On the other hand, when the hydrogen gas was removed, the oxygen  
 168 molecule in air reacts with the formed ionized hydrogen on the graphene and p-type silicon, which  
 169 increases the hole accumulation layer of graphene and decreases the ionized hydrogen in p-type  
 170 silicon, resulting in the final conductivity increase of the G-doped/p-Si.  
 171

#### 172 4. Conclusions

173 In this study, a graphene decorated porous silicon (G-doped/p-Si) substrate for low ppm H<sub>2</sub>  
174 gas detection by an inexpensive synthesis route was proposed, where the p-Si substrate with a large  
175 specific area was employed as a sensor matrix and graphene as a catalyst material. The H<sub>2</sub> sensing  
176 properties as a function of graphene concentration on the p-Si substrate were analyzed at room  
177 temperature. The G-doped/p-Si has an enhanced sensing property in comparison to that of pristine  
178 p-Si. The catalytic effect of graphene on the surface of p-Si was elucidated by enhancement in the  
179 carrier transfer to the adsorbed hydrogen gas molecules due to the doped graphene on the p-type  
180 silicon. The hierarchical hybrid structure of G-doping on porous silicone shows potential as an  
181 extended application of optical and medical sensors, and electronics for storage devices.  
182

183 **Supplementary Materials:** The following are available online at [www.mdpi.com/link](http://www.mdpi.com/link), Figure S1: (a) Optical  
184 microscope (OM) and (b) TEM images of the as-received graphene., Figure S2: (a) Surface and (b) cross-  
185 sectional morphology of porosity generated on the pristine Si substrate with an average thickness of 90  $\mu\text{m}$ .

186

187 **Acknowledgments:** his research was supported by Nano•Material Technology Development Program through  
188 the National Research Foundation of Korea (No. 2016M3A7B4900044) and Fundamental R&D Program for  
189 Core Technology of Materials (No. 10050890) funded by the Ministry of Science, ICT and Future Planning and  
190 Ministry of Trade, Industry & Energy, Republic of Korea.

191

192 **Author Contributions:** Nu Si A Eom and Hong-Baek Cho designed the project, collected data, analyzed and  
193 interpreted recorded data, and wrote the paper. Yoseb Song devised the hardware for gas sensing. Woojin Lee  
194 and Tohru Sekino helped the experiments and data collection. Yong-Ho Choa conceived and designed the  
195 experiments.

196

197 **Conflicts of Interest:** The authors declare no conflict of interest.

198

## 199 References

- 200 1. Anand, K.; Singh, O.; Singh, M.P.; Kaur, J.; Singh, R.C. Hydrogen sensor based on graphene/ZnO  
201 nanocomposite. *Sens. Actuators B Chem.*, **2014**, *195*, 409-415. DOI: 10.1016/j.snb.2014.01.029
- 202 2. Sayago, I.; Terrado, E.; Lafuente, E.; Horrillo, M.; Maser, W. K.; Benito, A.; Navarro, R.; Urriolabeitia, E.,  
203 Martinez, M., and Gutierrez, J., Hydrogen sensors based on carbon nanotubes thin films. *Synthetic Metals.*,  
204 **2005**, *148*, 15-19. DOI: 10.1016/j.synthmet.2004.09.013
- 205 3. Mubeen, S.; Zhang, T.; Yoo, B.; Deshusses, M.A.; Myung, N.V. Palladium nanoparticles decorated single-  
206 walled carbon nanotube hydrogen sensor. *J. Phys. Chem. C.*, **2007**, *111*, 6321-6327. DOI: 10.1021/jp067716m
- 207 4. Plecenik, A.; Haidry, A.; Plecenik, T.; Durina, P.; Truchly, M.; Mosko, M.; Grancic, B.; Gregor, M.; Roch, T.;  
208 Satrapinskyy, L., Metal oxide gas sensors on the nanoscale. 2014; pp. 90830Y-90830Y-90839. DOI:  
209 10.1117/12.2050349
- 210 5. Solntsev, V.; Litovchenko, V.; Gorbanyuk, T.; Evtukh, A., Influence of H<sub>2</sub>S and H<sub>2</sub> adsorption on  
211 characteristics of MIS structures with Si porous layers. *Semiconductor Physics, Quantum Electronics &*  
212 *Optoelectronics.*, **2008**, *11*, 381-384.
- 213 6. Korotcenkov, G. "Handbook of gas sensor materials," Properties, Advantages and and Shortcomings for  
214 Applications (2013). ISBN 978-1-4614-7165-3
- 215 7. Lundström, I.; Spetz, A.; Winqvist, F.; Ackelid, U.; Sundgren, H., Catalytic metals and field-effect  
216 devices—a useful combination. *Sens. Actuators B Chem.*, **1990**, *1*, 15-20. DOI:10.1016/0925-4005(90)80164-U
- 217 8. Gupta, D.; Dutta, D.; Kumar, M.; Barman, P.B.; Sarkar, C.K.; Basu, S.; Hazra, S.K., A low temperature  
218 hydrogen sensor based on palladium nanoparticles. *Sens. Actuators B Chem.*, **2014**, *196*, 215-222. DOI:  
219 10.1016/j.snb.2014.01.106

- 220 9. Emtsev, K.V.; Bostwick, A.; Horn, K.; Jobst, J.; Kellogg, G.L.; Ley, L.; McChesney, J.L.; Ohta, T.;  
221 Reshanov, S.A.; Röhrl, J., Towards wafer-size graphene layers by atmospheric pressure graphitization of  
222 silicon carbide. *Nat. Mater.*, **2009**, *8*, 203-207. DOI: 10.1038/NMAT2382
- 223 10. Novoselov, K.S.; Geim, A.K.; Morozov, S.; Jiang, D.; Katsnelson, M.; Grigorieva, I.; Dubonos, S.; Firsov,  
224 A., Two-dimensional gas of massless Dirac fermions in graphene. *Nature*, **2005**, *438*, 197-200. DOI:  
225 10.1038/nature04233
- 226 11. Xiang, C.; Jiang, D.; Zou, Y.; Chu, H.; Qiu, S.; Zhang, H.; Xu, F.; Sun, L.; Zheng, L., Ammonia sensor based  
227 on polypyrrole-graphene nanocomposite decorated with titania nanoparticles. *Ceram. Int.*, **2015**, *41*, 6432-  
228 6438. DOI: 10.1016/j.ceramint.2015.01.081
- 229 12. Peng, Y.; Ye, J.; Zheng, L.; Zou, K.;, The hydrogen sensing properties of Pt-Pd/reduced graphene oxide  
230 based sensor under different operating conditions. *Rsc Advances*, **2016**, *6*, 24880-24888. DOI:  
231 10.1039/C5RA26618A
- 232 13. Capone, S.; Forleo, A.; Francioso, L.; Rella, R.; Siciliano, P.; Spadavecchia, J.; Presicce, D.; Taurino, A.,  
233 Solid state gas sensors: state of the art and future activities. *Journal of Optoelectronics and Advanced*  
234 *Materials*, **2003**, *5*, 1335-1348. DOI: 10.3390/s90604323
- 235 14. Kong, J.; Franklin, N.R.; Zhou, C.; Chapline, M.G.; Peng, S.; Cho, K.; Dai, H.; Nanotube molecular wires as  
236 chemical sensors. *Science*, **2000**, *287*, 622-625. DOI: 10.1126/science.287.5453.622
- 237 15. Chourou, M.L.; Fukami, K.; Sakka, T.; Virtanen, S.; Ogata, Y.H., Metal-assisted etching of p-type silicon  
238 under anodic polarization in HF solution with and without H<sub>2</sub>O<sub>2</sub>. *Electrochimica Acta*, **2010**, *55*, 903-912.  
239 DOI: 10.1016/j.electacta.2009.09.048
- 240 16. Biswas S.; Drzal, L.T., Multilayered Nanoarchitecture of Graphene Nanosheets and Polypyrrole  
241 Nanowires for High Performance Supercapacitor Electrodes. *Chem. Mater.*, **2010**, *22*, 5667-5671. DOI:  
242 10.1021/cm101132g
- 243 17. Kim, J.; Oh, S.D.; Kim, J.H.; Shin, D.H.; Kim, S.; Choi, S.-H., Graphene/Si-nanowire heterostructure  
244 molecular sensors. *Scientific reports*, *4* (2014). DOI: 10.1038/srep05384
- 245 18. Novikov, D.S., Numbers of donors and acceptors from transport measurements in graphene. *Appl. Phys.*  
246 *Lett.*, **2007**, *91*, 102102. DOI: 10.1063/1.2779107
- 247 19. Riazimehr, S.; Bablich, A.; Schneider, D.; Kataria, S.; Passi, V.; Yim, C.; Duesberg, G.S.; Lemme, M.C.,  
248 Spectral sensitivity of graphene/silicon heterojunction photodetectors. *Solid State Electron.*, **2016**, *115*, Part  
249 B 207-212. DOI: 10.1016/j.sse.2015.08.023
- 250 20. Xie, C.; Lv, P.; Nie, B.; Jie, J.; Zhang, X.; Wang, Z.; Jiang, P.; Hu, Z.; Luo, L.; Zhu, Z., Monolayer graphene  
251 film/silicon nanowire array Schottky junction solar cells. *Appl. Phys. Lett.*, **2011**, *99*, 133113. DOI:  
252 10.1063/1.3643473